CrossMark

Charge injection barriers at metal/polyethylene interfaces

Lihua Chen[1] · Tran Doan Huan[1] · Yenny Cardona Quintero[1] · Rampi Ramprasad[1]

Abstract Charge injection barriers at metal/polymer interfaces are affected by many factors, including the physical, chemical, and electronic structure of the metal, the polymer, and the interfacial region. Here, we consider a diverse set of metals (Al, Ag, Au, Pd, and Pt), and a few metal/polyethylene interfacial configurations in an attempt to span situations encountered in real metal/polyethylene systems. Several relevant electronic properties and the charge injection barriers are computed for these cases using density functional theory computations. The calculations reveal important trends and correlations, and identify the favored mechanism of charge transport (as mediated by the charge injection barriers). While satisfactory correspondences of the computations with available measurements are achieved, quantitative discrepancies still remain between the computed and measured injection barriers. These issues may be resolved when more realistic models of the interface, inclusive of its morphological complexities, are utilized.

Introduction

Charge injection at metal/polymer interfaces in electrical systems such as capacitors and cables is believed to lead to progressive degradation, and ultimately, to the failure of

✉ Rampi Ramprasad
rampi.ramprasad@uconn.edu

Tran Doan Huan
huan.tran@uconn.edu

[1] Department of Materials Science and Engineering, Institute of Materials Science, University of Connecticut, 97 North Eagleville Road, Storrs, CT 06269, USA

the embedded polymer dielectric layers [1–5]. This process is governed by the electron and hole injection barriers (ϕ_e and ϕ_h), at the interface [1], which are, in principle, determined by the appropriate electronic properties of the metal (i.e., its work function), the dielectric (i.e., its band gap and electron affinity), and the interfacial region (i.e., its dipole moment) [1, 2].

Experimentally, ϕ_e and ϕ_h are typically (and directly) estimated by device-level current–voltage characteristics, and the pulsed electroacoustic method which relies on probing the (space) charge density profile across the interface [6]. Among metal/dielectric systems, polymer dielectrics pose enormous challenges to the unambiguous determination of the charge injection barriers. Despite their chemical simplicity, polymers display significant physical complexity—their morphology is composed of crystalline and amorphous regions, and the atomic-level structure at and close to the interface is composed of a diversity of bonding situations [7, 8]. Moreover, polymer dielectrics also contain chemical defects, e.g., occasional C=O (or carbonyl) groups instead of CH_2 units in polyethylene (PE) [9–11]. All these aspects affect the electronic structure across the metal/polymer interface. The measured ϕ_e and ϕ_h naturally include the effects of the complexities alluded to above. Unraveling the specific roles of the various relevant factors in determining ϕ_e and ϕ_h is thus far from trivial.

Determining ϕ_e and ϕ_h for *realistic* metal/polymer interfaces using density functional theory (DFT) calculations is also in a state of infancy [12, 13]. It is worth noting that the theory to determine ϕ_e and ϕ_h, given the interfacial atomic-level structure, is indeed available. In fact, for cases where the interface structure is much less complex than in metal/polymer interfaces (such as GaAs/AlAs [14], HfO_2/metal [15–19], high-k oxide/Si [20–22], etc.), ϕ_e, ϕ_h as

well as the effective work function (a related quantity) have been computed with acceptable accuracy.

The essential ingredients necessary to compute ϕ_e and ϕ_h for a metal/insulator system include the work function of the metal (ψ_m), the band gap (E_g), and the electron affinity (E_{ea}) of the insulator, and the interfacial dipole moment-induced vacuum level shift ($\Delta\varphi$). Note that, barring the last quantity (namely, $\Delta\varphi$), the other properties are those of the individual systems that make up the interface. The dipole moment is intimately tied to the interfacial structure and bonding. A lack of knowledge (or an incorrect assumption) of the nature of the interface will lead to errors in the prediction of the dipole moment, and hence ϕ_e and ϕ_h.

In the present work, we compute ϕ_e and ϕ_h of metal/PE interfaces using DFT, with the metal being Al, Ag, Au, Pd, or Pt (which are conventional choices for practical and model electrodes). This selection of metals also spans a large range of work function values. Three different geometries of contact between PE and the metal were considered, in an attempt to span a few extreme cases of interface configurations. Each of the computed quantities—namely, ψ_m, E_g, and E_{ea} of PE, and $\Delta\varphi$ at the metal/PE interface—compares well with available experimental data. Trends in the computed ϕ_e and ϕ_h values, and the (lack of) variation of ϕ_e and ϕ_h with the metal work function are also in favorable agreement with measurements. Nevertheless, the predicted barriers are only in semi-quantitative agreement with the limited available measurements, indicating the need for more realistic models of the metal/PE interface (inclusive of morphological complexity and chemical defects). We hope that such information may be provided by physical and electrical characterization of metal/polymer interfaces in the future.

This paper is organized as follows. "Models and methods" section presents the details of the interface models and the computational methodology. In "Results and discussion" section, we discuss the calculations of ψ_m, $\Delta\varphi$, E_{ea}, and E_g, and finally, ϕ_e and ϕ_h. "Conclusions" section summarizes the obtained results and proposes some suggestions for future work.

Models and methods

Models

Metal/PE interface models were constructed by placing a PE slab on a (111) metal slab (see Fig. 1). The metal slab consisted of nine atomic layers, with the metal being Al, Ag, Au, Pd, or Pt. We considered three different configurations of the PE slab, referred to as PE$_{(001)}$, PE$_{(110)}$, and
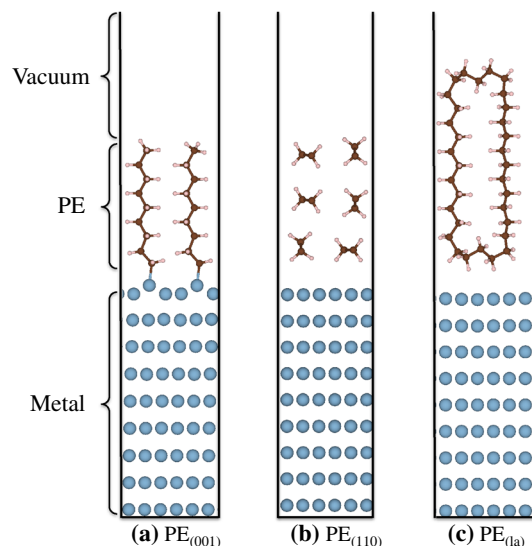

Fig. 1 Geometries of the metal/PE interfaces considered. Metal, carbon, and hydrogen atoms are shown in *blue*, *dark-brown,* and *pink*, respectively. PE chains are normal to the metal surface (**a**, PE$_{(001)}$), parallel to the surface (**b**, PE$_{(110)}$), and are folded next to the surface (**c**, PE$_{(la)}$) (Color figure online)

PE$_{(la)}$, wherein the subscript indicates the orientation of the $-CH_2-$ chains of crystalline PE. For PE$_{(001)}$ and PE$_{(110)}$, the $-CH_2-$ chains are normal to and parallel with the metal surface, respectively. PE lamellae, a typical variant of PE whose chains adopt a variety of formats, e.g., curves and fragments [7], are modeled by PE$_{(la)}$ in which these chains are folded, approaching the metal surface from different angles. The number of PE layers used in the PE$_{(001)}$, PE$_{(110)}$, and PE$_{(la)}$ slabs was 9, 3, and 11, respectively. The in-plane lattice dimensions of the PE slab were slightly strained by a few percent to match with the metal lattice constant at the interface. A vacuum layer of 14 Å was used to suppress the interactions between the system and its periodic images.

Charge injection barriers

Schematics of the energy diagram of a metal/PE interface are portrayed in Fig. 2. Before contact, the isolated PE and metal slabs share the same vacuum level. When the two materials are contacted, an electric dipole **D** pointing across the interface is created, misaligning the vacuum level of one material with respect to the other by $\Delta\varphi$, which can be expressed as [16, 23]

$$\Delta\varphi = -\frac{e|\mathbf{D}|}{\varepsilon_0 A}. \tag{1}$$

Here, ε_0 is the vacuum permittivity, e is an electron charge, and A is the area of the interface.
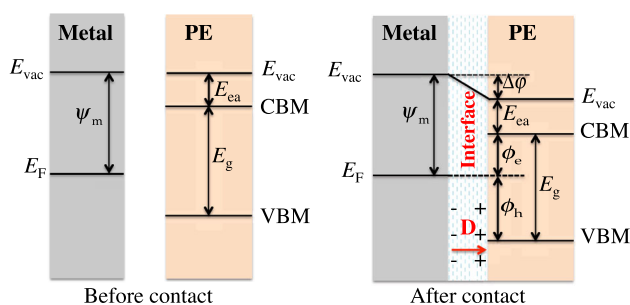
Fig. 2 Energy diagram of a metal/PE interface, before (**a**) and after (**b**) physical contact, where E_F, E_{vac}, and CBM and VBM are the metal Fermi level, vacuum level, and the conduction band minimum and valence band maximum of PE, respectively. Due to the interfacial dipole moment **D** created after physical contact between the metal and PE, the vacuum levels of the two materials are misaligned by $\Delta\varphi$. Based on ψ_m, E_g, E_{ea}, $\phi_e = \psi_m - E_{ea} - \Delta\varphi$ and $\phi_h = E_g - \phi_e$

Assuming that the metal work function ψ_m, the vacuum level shift $\Delta\varphi$, the PE electron affinity E_{ea}, and band gap E_g are available, ϕ_e is given by

$$\phi_e = \psi_m - E_{ea} - \Delta\varphi. \tag{2}$$

ϕ_h can be computed as

$$\phi_h = E_g - \phi_e. \tag{3}$$

All the quantities needed to determine ϕ_e and ϕ_h, i.e., ψ_m, $\Delta\varphi$, E_{ea}, and E_g, can be calculated with DFT, as demonstrated in "Results and discussion" section. We note that apart from $\Delta\varphi$, the other quantities (namely, ψ_m, E_{ea}, and E_g) are properties of the individual materials that make up the interfacial system.

Calculations details

The properties of the metal, PE, and metal/PE interfaces were calculated using first-principles computations within the framework of DFT [28, 29] as implemented in the Vienna *Ab-initio* Simulation Package (VASP). The generalized gradient approximation Perdew–Burke–Ernzerhof (PBE) [30] functional for the exchange-correlation (XC) energies and a plane wave energy cutoff of 400 eV for the basis set were used. In calculations with bulk metals and crystalline PE, dense Monkhorst-Pack **k**-point meshes of $14 \times 14 \times 14$ and $4 \times 4 \times 10$, respectively, were used to sample their Brillouin zones. For the interface models, the **k**-point mesh was $4 \times 4 \times 1$. van der Waals interactions, known to be important in stabilizing polymers like PE [31], were included using the non-local density functional vdW-DF2 [32]. Atomic coordinates were relaxed until atomic forces were smaller than 0.01 eV/Å. The optimized lattice parameters of the bulk metals and PE crystal are listed in Table 1, showing an excellent agreement with experiment data.

Table 1 Optimized lattice parameters a, b, and c of the orthorhombic *Pnma* PE crystal and a of the cubic $Fm\overline{3}m$ Ag, Au, Al, Pd, and Pt crystals, all given in Å

System	Lattice constants			Work function		
	This work	Expt.	Ref.	This work	Expt.	Ref.
PE						
a	7.00	7.12	[24]			
b	4.86	4.85	[24]			
c	2.56	2.55	[24]			
Al						
a	4.05	4.05	[25]	4.05	4.26	[26]
Ag						
a	4.15	4.09	[25]	4.43	4.74	[26]
Au						
a	4.16	4.08	[25]	5.21	5.31	[26]
Pd						
a	3.94	3.89	[27]	5.30	5.60	[26]
Pt						
a	3.97	3.92	[25]	5.70	5.93	[26]

The calculated metal work function is given in eV. For validation, relevant experimental data are also provided

Because $\phi_e + \phi_h = E_g$, it is crucial to correctly calculate E_g in order to determine one of the two barriers, given the other. Moreover, the band edge positions are also required to be properly captured so that quantities such as E_{ea} can be computed accurately. Calculations at the PBE level of theory systematically underestimate insulator band gap by 30 % or more, and lead to uncertainties in the positions of the band edges [33, 34]. In the case of PE, we obtained a band gap of 6.68 eV with PBE, while the measured band gap of this polymer is 8.80 eV [35]. The state-of-the-art treatment for computing E_g accurately is the GW method, which is based on many-body perturbation theory [36]. Compared to calculations with PBE, *GW* calculations are far more expensive but the calculated band gap and band edge positions are significantly more accurate. Here, we calculated the PE band gap as 8.72 eV with G_0W_0, a version of *GW* as implemented in VASP. This calculated value agrees well with the true band gap of PE [35], and was used for our calculations of E_{ea}, ϕ_e, and ϕ_h.

Results and discussion

As is evident from the discussion in "Charge injection barriers" section, and Eqs. (2) and (3), computation of the charge injection barrier requires a knowledge of the ψ_m, E_{ea}, E_g, and $\Delta\varphi$ for the appropriate systems considered here. Below, we present our results for each of these

quantities (with the exception of E_g, which was discussed above), and use them to evaluate the charge injection barriers for the metal/PE interfaces.

The metal work function ψ_m

The energy needed to remove an electron from a metal, or the work function ψ_m, can be calculated as the difference between the metal Fermi level and the metal vacuum level, as shown in Fig. 2. The standard method which has widely been used [15, 37] to calculate ψ_m, referred to as the "bulk plus band lineup" method [14, 38], involves several steps. First, the energy difference between the average effective potential (experienced by the electrons) and the Fermi energy of the bulk metal system is calculated. Then, calculations for a metal slab with appropriate orientation are performed, determining the average effective potential deep inside the metal slab (i.e., sufficiently far from the surface), as well as the position of the vacuum level. Finally, the energy difference obtained in the first step is used to place the Fermi level with respect to the vacuum level. We show in Table 1 the work function calculated for Al, Ag, Au, Pd, and Pt. Calculated results are within 5 % of the experimentally measured data, indicating that our DFT-based computational scheme is reasonable for determining ψ_m.

The PE electron affinity E_{ea}

The electron affinity E_{ea} needed in Eq. (2) for PE is the energy difference between the vacuum level and the conduction band minimum (CBM) of PE. To determine CBM with respect to the vacuum level, the "bulk plus band lineup" procedure described above was used. The electron affinities of the $PE_{(110)}$, $PE_{(la)}$, and $PE_{(001)}$ slabs (with the band edges of bulk PE calculated with G_0W_0 method) are found to be -1.33 eV, -1.23 eV, and -1.16 eV, respectively. These results agree well with the experimentally measured E_{ea} that ranges between -1.20 eV and 0 eV [35].

The metal/PE dipole-induced vacuum level shift $\Delta\varphi$

Interfacial effects like charge transfer are ubiquitous in heterostructures, leading to the *interface-originated* vacuum level shift $\Delta\varphi$ (see Fig. 2). Starting from the DFT charge density, the electric dipole **D** appearing in Eq. (1) was determined by integrating the elementary dipole moment over the whole total volume of the system. Calculated results for the dipole-induced $\Delta\varphi$ are shown in Table 2. We note that only the $\Delta\varphi$ of $Al/PE_{(001)}$ takes a positive value, compared with other metal/$PE_{(001)}$ interfaces. This is because the vacuum energy shift is originated

Table 2 Calculated vacuum level shift $\Delta\varphi$ of the metal/PE interfaces, given in eV

System	$PE_{(001)}$	$PE_{(la)}$	$PE_{(110)}$	Expt.
Al-PE	0.29	-0.19	-0.20	-0.30
Ag-PE	-0.20	-0.56	-0.59	-0.50
Au-PE	-1.18	-0.48	-0.58	-0.70
Pd-PE	-1.26	-0.43	-0.72	N/A
Pt-PE	-1.45	-0.59	-0.61	N/A

Experimental data is taken from Ref. [39] for the metal/TTC interface, which is similar to the metal/$PE_{(110)}$ interface. See text for further details.

from the charge transfer process which is primarily mediated by the metal-carbon bonds formed at the interface. While Al may donate electrons (from the 3s and 3p shells), the other transition metals prefer to gain more electrons for closing their d shell. This difference leads to charge transfer, and ultimately, vacuum energy shifts, in opposite directions. To the best of our knowledge, similar data for metal/PE interfaces are unavailable. Therefore, for validation purposes, our results were compared with $\Delta\varphi$ measured for the interfaces between tetratetracontane [TTC-nCH$_3$(CH$_2$)$_{42}$CH$_3$] and Al, Ag, and Au [39, 40]. A comparison between the measured metal/TTC and the modeled metal/$PE_{(110)}$ interfaces is justified because their structures are somewhat similar, i.e., the TTC molecules was found to lie parallel to the metal surface [40]. Indeed, the calculated and measured $\Delta\varphi$ are consistent, suggesting that the results of our calculation methodology for $\Delta\varphi$ at the metal/PE interfaces are appropriate for estimating the charge injection barriers using Eqs. (2) and (3). Nevertheless, we note that the interfacial structure of real metal/PE interfaces may be more complex than the models used here.
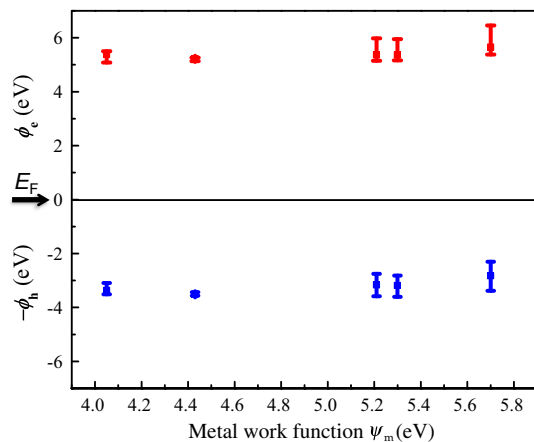
Electron and hole injection barriers (ϕ_e and ϕ_h) at metal/PE interface

Given the ψ_m, E_{ea}, E_g, and $\Delta\varphi$ calculated by DFT, ϕ_e and ϕ_h were determined. The obtained results are shown in Table 3. For ease of visualization, these results are also plotted in Fig. 3. For each choice of metal, both ϕ_e and ϕ_h are shown. The error bars in Fig. 3 represent the spread in the values due to the choice of the interface geometry.

Several observations can be made based on the results captured in Fig. 3. First, it is evident that the charge injection barriers do not follow a clear relationship with the metal work function. For instance, although Al and Pt are, respectively, the metals with the lowest and highest work function values, they do not necessarily lead to the lowest

Table 3 The computed ϕ_e and ϕ_h of the metal/PE interfaces with $E_g^{G_0W_0}$, given in eV

System	ϕ_e			ϕ_h		
	$PE_{(110)}$	$PE_{(la)}$	$PE_{(001)}$	$PE_{(110)}$	$PE_{(la)}$	$PE_{(001)}$
Al/PE	5.39	5.08	5.50	3.33	3.64	3.22
Ag/PE	5.20	5.13	5.26	3.52	3.59	3.46
Au/PE	5.98	5.91	5.19	2.74	2.81	3.53
Pd/PE	5.95	5.82	5.20	2.77	2.90	3.52
Pt/PE	6.46	6.35	5.40	2.26	2.37	3.32

Fig. 3 ϕ_e and ϕ_h (denoted by *red* and *blue* colors, respectively) of the metal/PE interfaces versus ψ_m. The Fermi energy (E_F) of all metal is set as 0. The *error bars* represent the spread in the barrier height values arising from the choice of the interface geometries (based on the data contained in Table 3) (Color figure online)

and highest charge injection barriers. This aspect is indeed consistent with previous measurements [5], and understandable, because the injection barriers are determined by the combined effects of the metal work function and the vacuum level shift due to the interface dipole moment. Furthermore, for a given metal/PE system, the barriers can be significantly modulated by the details of the interface geometry, as captured by the error bars in Fig. 3, which further diminish the variations in the barriers between different metal/PE systems. These observations allow us to appreciate the important role played by the interface; this can potentially outweigh the effects of the metal work function.

Second, the computed ϕ_h and ϕ_e are, respectively, in the 2.26–3.64 eV and 5.08–6.46 eV ranges. The ϕ_h is thus consistently smaller than ϕ_e, indicating that in the cases considered here, hole conduction will dominate. This phenomenon was previously anticipated via the measurements of the net charge density accumulated in Ag/PE films [5], suggesting that the positive charge injection was more favored under high electric field.

Finally, the predicted barriers are only in semi-quantitative agreement with the limited available measurements.

Current–voltage measurements for Al/PE systems imply a barrier height of 2.14 eV [41] which is in reasonable agreement with the predicted ϕ_h value for the same system. However, more recent measurements for a variety of metal electrodes indicate the charge injection barriers of about 1 eV [2]. The rather partially satisfactory correspondence between computations and measurements for the charge injection barriers is indicative of the possible difference between the interface model simulated and the real complex situation. In other words, more accurate charge injection barriers can only be predicted when more realistic models of the metal/PE interface, incorporating complex morphological details, appropriate atomic binding modes and chemical defects, are captured in the computations.

Conclusions

An attempt has been made to understand the role of various electronic, physical, and chemical factors in controlling the charge (electron or hole) injection barriers at metal/polymer interfaces, via density functional theory calculations. A variety of metals, including Al, Ag, Au, Pd, and Pt, and a few metal/PE interface models were considered. Computing the charge injection barrier requires the following ingredients: the metal work function, the PE band gap and electron affinity, and the vacuum level shift induced by the interface dipole moment. Of these, the vacuum level shift is intimately controlled by the interfacial structure and bonding, while all the other properties are those of the individual systems that make up the interface.

The present investigation has lead to important trends concerning the charge injection barrier. We find that the injection barrier is not a strong function of the metal work function, but is rather determined by the combined effect of the metal work function and the vacuum shift due to the interfacial dipole (which, in turn, is determined by the details of the structure and bonding at the interface). Al, with the lowest work function (of the metals considered here), does not necessarily lead to the smallest barrier, nor does Pt, with a highest work function, display the largest barrier. Moreover, the calculated hole injection barriers are considerably smaller than the electron injection barriers of the same interface, implying that in these interfaces, the hole injection process is dominant. All of these trends, as well as the computed properties of each material, are consistent with the experiments. With respect to the actual values of the charge injection barriers themselves, the computed quantities are overestimated with respect to the available estimates from current–voltage measurements. These discrepancies suggest that more realistic metal/PE interface models, inclusive of the morphological complexity and chemical defects known to be present at

interfaces, should be considered in the computations. It is hoped that such critical information will be provided by detailed physical and electrical characterization of metal/polymer interfaces in the future.

Compliance with ethical standards

Conflict of interest The authors declare that they have no conflict of interest.

References

1. Dissado LA, Fothergill JC (1992) Electrical degradation and breakdown in polymers. IET, London
2. Teyssedre G, Laurent C (2005) Charge transport modeling in insulating polymers: from molecular to macroscopic scale. IEEE Trans Dielectr Electr Insul 12:857–875
3. Mizutanim T (2005) Behavior of charge carriers near metal/polymer interface. In: Proceedings of the 2005 international symposium on electrical insulating materials, Japan, pp 1–6
4. Tanaka T (2001) Space charge injected via interfaces and tree initiation in polymers. In: IEEE conference on electrical insulation and dielectric phenomena, Kitchener, Ont, pp 1–15
5. Taleb M, Teyssèdre G, Le Roy S (2009) Role of the interface on charge build-up in a low-density polyethylene: surface roughness and nature of the electrode. In: IEEE conference on electrical insulation and dielectric phenomena, pp 112–115
6. Li Y, Yasuda M, Takada T (1994) Pulsed electroacoustic method for measurement of charge accumulation in solid dielectrics. IEEE Trans Dielectr Electr Insul 1:188–195
7. Peacook AJ (2000) Handbook of polyethylene: structures: properties, and applications. Taylor & Francis, New York
8. Ungar G (1981) Radiation effects in polyethylene and n-alkanes. J Mater Sci 16:2635–2656. doi:10.1007/BF02402826
9. Odak D, Kaczmarek H, Buffeteau T, Sourisseau C (2005) Photo- and bio-degradation processes in polyethylene, cellulose and their blends studied by ATR-FTIR and Raman spectroscopies. J Mater Sci 40:4189–4198. doi:10.1007/s10853-005-2821-y
10. Huzayyin A, Boggs S, Ramprasad R (2010) Density functional analysis of chemical impurities in dielectric polyethylene. IEEE Trans Dielectr Electr Insul 17:926–930
11. Huzayyin A, Boggs S, Ramprasad R (2010) Quantum mechanical studies of carbonyl impurities in dielectric polyethylene. IEEE Trans Dielectr Electr Insul 17:920–925
12. Huzayyin A, Boggs S, Ramprasad R (2011) Quantum mechanical study of charge injection at the interface of polyethylene and platinum. In: IEEE conference on electrical insulation and dielectric phenomena, Cancun, pp 800–803
13. Chen LH, Huan TD, Huzayyin A, Quintero Y, Ramprasad R (2014) First-principles study of aluminum-polyethylene interfaces. In: IEEE conference on electrical insulation and dielectric phenomena, Des Moines, IA, pp 887–890
14. Van de Walle CG, Martin RM (1987) Theoretical study of band offsets at semiconductor interfaces. Phys Rev B 35:8154–8165
15. Uttamchandani R, Zhang X, Shankar S, Lu G (2015) Chemical tuning of band alignments for Cu/HfO_2 interfaces. Phys Status Solidi b 252:298–304
16. Zhu H, Ramprasad R (2011) Effective work function of metals interfaced with dielectrics: a first-principles study of the $Pt-HfO_2$ interface. Phys Rev B 83:081416
17. Zhu H, Tang C, Fonseca LRC, Ramprasad R (2012) Recent progress in ab initio simulations of hafnia-based gate stacks. J Mater Sci 47:7399–7416. doi:10.1007/s10853-012-6568-y
18. Zhu H, Ramanath G, Ramprasad R (2013) Interface engineering through atomic dopants in HfO_2-based gate stacks. J Appl Phys 114:114310
19. Mukhopadhyay AB, Sanz JF, Musgrave CB (2010) Effect of interface structure on the Ru on HfO_2 work function. J Mater Sci 45:4924–4928. doi:10.1007/s10853-010-4274-1
20. Shaltaf R, Rignanese GM, Gonze X, Giustino F, Pasquarello A (2008) Band offsets at the $SiSiO_2$ interface from many-body perturbation theory. Phys Rev Lett 100:186401
21. Puthenkovilakam R, Chang JP (2004) An accurate determination of barrier heights at the HfO_2/Si interfaces. J Appl Phys 96:2701–2707
22. Puthenkovilakam R, Chang JP (2004) Valence band structure and band alignment at the ZrO_2/Si interface. Appl Phys Lett 84:1353–1355
23. Cardona QY, Zhu H, Ramprasad R (2013) Adsorption of CH_3S and CF_3S on Pt(111) surface: a density functional theory study. J Mater Sci 48:2277–2283. doi:10.1007/s10853-012-7005-y
24. Avitabile G, Napolitano R, Pirozzi B, Rouse KD, Thomas MW, Willis BTM (1975) Low temperature crystal structure of polyethylene: results from a neutron diffraction study and from potential energy calculations. J Polym Sci Polym Lett Ed 13:351–355
25. Kittel C (2004) Introduction to solid state physics, 8th edn. Wiley, New York
26. Haynes WM (2012) CRC handbook of chemistry and physics. CRC Press, Boca Raton
27. Todorova M, Reuter K, Scheffler M (2004) Oxygen overlayers on Pd (111) studied by density functional theory. J Phys Chem B 108:14477–14483
28. Hohenberg P, Kohn W (1964) Inhomogeneous electron gas. Phys Rev 136:B864–B871
29. Kohn W, Sham LJ (1965) Self-consistent equations including exchange and correlation effects. Phys Rev 140:A1133–1138
30. Perdew JP, Burke K, Ernzerhof M (1996) Generalized gradient approximation made simple. Phys Rev Lett 77:3865–3868
31. Liu CS, Pilania G, Wang CC, Ramprasad R (2012) How critical are the van der Waals interactions in polymer crystals? J Phys Chem A 116:9347–9352
32. Lee K, Murray ÉD, Kong L, Lundqvist BI, Langreth DC (2010) Higher-accuracy van der Waals density functional. Phys Rev B 82:081101
33. Hybertsen MS, Louie SG (1985) First-principles theory of quasiparticles: calculation of band gaps in semiconductors and insulators. Phys Rev Lett 55:1418–1421
34. Perdew JP (1985) Density functional theory and the band gap problem. Int J Quant Chem 28:497–523
35. Less KJ, Wilson EG (1973) Intrinsic photoconduction and photoemission in polyethylene. J Phys C 6:3110–3120
36. Hedin L (1965) New method for calculating the one-particle Green's function with application to the electron-gas problem. Phys Rev 139:A796–A823
37. Ramprasad R, von Allmen P, Fonseca L (1999) Contributions to the work function: a density-functional study of adsorbates at graphene ribbon edges. Phys Rev B 60:6023–6027
38. Ramprasad R, Shi N, Tang C (2010) Dielectric polymer nanocomposites. Springer, New York, pp 133–161
39. Ishii H, Sugiyama K, Ito E, Seki K (1999) Energy level alignment and interfacial electronic structures at organic/metal and organic/organic interfaces. Adv Mater 11:605–625

40. Ito E, Oji H, Ishii H, Oichi K, Ouchi Y, Seki K (1998) Interfacial electronic structure of long-chain alkane/metal systems studied by UV-photoelectron and metastable atom electron spectro-scopies. Chem Phys Lett 287:137–142

41. Taylor DM, Lewis TJ (1971) Electrical conduction in poly-ethylene terephthalate and polyethylene films. J Phys D 4:1346–1357